DOCTORAL THESIS

Enhancement of radiofrequency ablation of the liver combined with transarterial embolization using various embolic agents

(動脈塞栓術を併用したラジオ波焼灼療法における塞栓物質の違いと焼灼域拡大効果の検討)

March, 2017（2017 年 3 月）

Kuniyasu Irie

入江　邦泰

Gastroenterology

Yokohama City University Graduate School of Medicine

横浜市立大学 大学院医学研究科 医科学専攻 消化器内科学

（ Doctoral Supervisor：Shin Maeda, Professor ）

（ 指導教員：前田　愼 教授 ）

Abdominal Imaging

Published online: 21 December 2014

Abdom Imaging (2015) 40:1821–1828
DOI: 10.1007/s00261-014-0332-5

Enhancement of radiofrequency ablation of the liver combined with transarterial embolization using various embolic agents

Kuniyasu Irie,[1] Manabu Morimoto,[1,2] Kazushi Numata,[2] Masaaki Kondo,[2] Satoshi Moriya,[3] Yu Shimoyama,[2] Akito Nozaki,[2] Yoshihiro Goda,[1] Satoshi Kobayashi,[1] Makoto Ueno,[1] Shinichi Ohkawa,[1] Katsuaki Tanaka,[2] Shin Maeda[3]

[1]Department of Hepatobiliary and Pancreatic Oncology, Kanagawa Cancer Center, 2-3-2 Nakao, Asahi-ku, Yokohama 241-8515, Japan
[2]Gastroenterological Center, Yokohama City University Medical Center, Yokohama, Japan
[3]Division of Gastroenterology, Yokohama City University Graduate School of Medicine, Yokohama, Japan

Abstract

Purpose: Reducing blood flow in the liver during radiofrequency ablation causes enlargement of the ablation area. In this animal study, we evaluated the extended effects of radiofrequency ablation combined with transarterial embolization using various embolic agents.
Methods: We treated 38 radiofrequency ablation lesions after embolization in 13 pigs using the following embolic agents: gelatin sponge (Group A); iodized oil followed by gelatin sponge (Group B); 700–900 μm calibrated microspheres (Group C); and 100–300 μm calibrated microspheres (Group D). Lesion size and pathological evaluations of these ablation lesions were compared with those receiving radiofrequency ablation alone (control).
Results: Both the long- and short-axis diameters of the ablation lesions for Groups A, B, C, and D were significantly longer than those of controls (long axis/short axis for Groups A, B, C, D, and controls were 27.2/23.2, 30.2/26.0, 28.2/22.2, 32.0/24.4, and 23.2 mm/18.5 mm, respectively) ($P < 0.05$). The long-axis of the ablation lesion for Group D was significantly longer than those for both Groups A and C ($P < 0.05$). At pathological examination, the central ablation lesions showed coagulative necrosis with a surrounding hemorrhagic rim, and the microspheres were fitted to occlude the small arteries in peripheral liver parenchyma in Groups C and D.
Conclusions: The extended effects of embolization with small microspheres may be stronger than those with large microspheres and were equal to those with iodized oil followed by gelatin sponge.

Key words: Radiofrequency—Embolization—Microspheres—Hepatocellular carcinoma—Coagulation—Combination

Surgical resection and liver transplantation are considered the most effective treatment options for patients with hepatocellular carcinoma (HCC); however, many patients are not suitable candidates for surgical treatment because of the extent of the tumor burden, poor liver function reserve, and/or a shortage of donors [1]. Radiofrequency ablation has achieved attention as a minimally invasive technique for the local treatment of HCC and has been developed as an alternative to surgical treatment [2, 3]. Radiofrequency ablation has been shown to provide complete necrosis in 76%–100% of tumors smaller than 3 cm in diameter [4, 5]; however, in tumors larger than 3 cm, the percentage of complete necrosis varied between 29% and 70% because of a limited region of coagulative necrosis induced by radiofrequency ablation [5, 6]. Tumor size affects the efficacy of the ablation, because of the so-called "heat-sink" effect by blood flow adjacent to the liver parenchyma and is the main limitation for radiofrequency ablation of liver tumors [7]. To improve these ablation-induced thermal effects, animal and human studies have attempted to reduce the blood supply during ablation by various procedures, such as temporary occlusion of the tumor

Correspondence to: Manabu Morimoto; *email:* m-morimoto@kcch.jp

blood supply [8, 9], chemoembolization, and embolization [10, 11]. Transarterial chemoembolization has been performed for the treatment of unresectable HCC by combining the effects of targeted chemotherapy with those of ischemic necrosis [12, 13]. The use of iodized oil in embolization procedures allows a more effective targeting of HCC and the dual embolization of the hepatic artery and portal venules supplying the HCC [14]. Previous studies in animal models have shown that radiofrequency ablation combined with embolization using iodized oil and a gelatin sponge induced the greatest area of coagulative necrosis among the various embolization procedures; moreover, the ablated zone was accompanied by a peripherally spreading segmental hemorrhagic area [15].

Recently, small, calibrated microspheres have been commercially available [16]. Although some preliminary studies of radiofrequency ablation combined with embolization using the microspheres have been reported [17, 18], the ablation-induced thermal effects of the various embolic agents have not been clarified. The aim of this animal study was to evaluate the extended effects of radiofrequency ablation combined with transarterial embolization using various embolic agents.

Materials and methods

Animals and animal care

Approval from the institutional committee for the care of research animals was obtained before the start of the study. A total of 13 juvenile female domestic pigs weighing 55–68 kg (mean 61 kg) were used. Two or three pigs were assigned to each of the following five embolization procedures before radiofrequency ablation: Group A, embolization with gelatin sponge; Group B, embolization with iodized oil followed by gelatin sponge; Group C, embolization with 700–900 μm calibrated microspheres; Group D, embolization with 100–300 μm calibrated microspheres; and the non-embolized control group. After intramuscular premedication with xylazine (5 mg/kg) and ketamine (5 mg/kg), anesthesia was induced. All animals were received tracheal intubation and were mechanically ventilated with 1.3% end-tidal halothane in oxygen (50%) and nitrous oxide (50%). Cardiac and respiratory parameters were monitored throughout the procedures. Open laparotomy was performed through a midline incision to exteriorize the liver for embolization and radiofrequency ablation.

Embolization procedure

All interventional procedures were performed with a mobile C-arm-based angiography system. For angiographic procedures, a 5-F introducer sheath (Pinnacle introducer; Terumo, Tokyo, Japan) was inserted into the right femoral artery through a cut-down to allow access without substantial blood loss. Under fluoroscopic guidance, a 4-F cobra-shaped angiographic catheter (Terumo, Tokyo, Japan) was inserted into the celiac trunk and the hepatic artery, and digital subtraction angiography was performed by injecting iodinated contrast medium. Embolization was performed by selectively introducing a catheter into the common hepatic artery and injecting embolic agents.

In Group A, embolization was performed using a gelatin sponge (1 × 1 × 1 mm) (Gelpart; Nippon Kayaku, Tokyo, Japan). Eighty milligrams of gelatin sponge suspended in 8 mL of iodinated contrast was injected until the second branch of the hepatic arteries disappeared. In Group B, embolization was performed with a gelatin sponge after introducing 8–10 mL of iodized oil (Lipiodol; Andre Guerbet, Aulnay-sous-Bois, France) until the oil entered the intrahepatic branch of the portal vein. In Groups C and D, embolization with calibrated 700–900 μm (Group C) or 100–300 μm (Group D) microspheres (Embosphere; Nippon Kayaku, Tokyo, Japan) was performed. A vial of the microspheres suspended in 9 mL of carrier solution was mixed with 9 mL of iodinated contrast medium. The suspended microspheres were then slowly injected with a 1-mL syringe. The end point of embolization with microspheres was disappearance of the flow in the targeted hepatic arterial branch [19, 20]. After all procedures, the catheter and the introducer sheath were removed.

Radiofrequency ablation procedure

Immediately after the embolization procedures, radiofrequency ablation was performed. After four grounding pads were placed on the animal's back, a probe and the grounding pads were connected with a commercially available monopolar radiofrequency generator (RF 3000; Boston Scientific, Natick, MA, USA). A single 15-gage, 2-cm expandable eight-hook needle electrode (LeVeen needle electrode; Boston Scientific, Natick, MA, USA) was inserted into the liver under ultrasound guidance, and the hooks were deployed. Four electrode insertions were performed per pig; one of each of the right internal liver lobe, right lateral liver lobe, left internal liver lobe, and left lateral liver lobe to prevent potential overlaps in ablation areas induced by the two separate radiofrequency applications. After verifying the position of the needle, the ablation was initiated. A two-phase application process was performed. In the first phase, the initial generator output was set at 30 W for 1 min and then increased by 10 W every minute until the power output reached 60 W. The output was maintained at 60 W for 10 min or until circuit impedance increased to more than 200 Ω (i.e., "roll-off"), at which time the power output was decreased until the baseline impedance was reached. After a 30-s interval, the second phase was performed at half of the first phase. After 5 min, the power was increased by

10 W/min up to a maximum of 60 W. Radiofrequency ablation was finished when the second roll-off occurred. In all experiments, the power, current, and impedance were recorded at baseline and at 15-s intervals thereafter. The total radiofrequency application time was calculated as the sum of the duration of the first and second phases of ablation. Fifty-two radiofrequency ablation lesions were made in a total of 13 pigs.

Lesion size and pathologic analysis

After radiofrequency ablation, the animals were humanely euthanized with an overdose (25 mL) of potassium chloride solution (Shimizu Pharmaceutical, Shizuoka, Japan), and the livers were removed for gross and pathological analysis. The liver was cut into 0.5 cm serial sections in a cross-sectional fashion perpendicular to the line of the radiofrequency ablation electrode tract. If the ablation lesion was bulging out of the liver surface at gross examination, the lesion was not collected for examination, because the lesion size could not be measured accurately. The measurements for the diameter of the area of coagulation perpendicular to the electrode axis, the length of the area of coagulation along the electrode tract, and the width of the hemorrhagic rim were obtained by consensus of two observers who were blinded to the treatment modality. Circularity was calculated to describe the roundness of the ablation zones as described previously [21]: circularity = (short axis)/(long axis). The liver was fixed in a buffered 10% formalin solution. After complex fixation for at least 24 h, the liver was sectioned axially in 5 mm cuts. Tissue samples were embedded in paraffin and cut into 2–3 μm sections and placed on glass sides. After rehydration, the sections were stained with hematoxylin and eosin for microscopic examination.

Statistical analysis

All data are expressed as mathematical mean ± standard deviation and were statistically analyzed by analysis of variance. The Bonferroni test was performed to analyze the coagulation diameters, the diameters of the marginal rim, and radiofrequency application times among the groups with positive F values. Bivariate correlations between the dimensions of the hemorrhagic rim and the long-axis of the ablation lesions were statistically evaluated using the Pearson's correlation coefficient. Statistical significance was set at $P < 0.05$. Statistical analyses were performed using SPSS version 21 for Windows (IBM SPSS, Chicago, IL, USA).

Results

For all animals, cardiac and respiratory parameters remained stable throughout the treatment procedures. A total of 52 treatment lesions were successfully performed without any complications during the procedure, and 38 of those could be evaluated for lesion size and pathological examinations.

Lesion size

The ablation area could be easily distinguished from the surrounding normal liver tissue. The long- and short-axis diameters and average diameters of the marginal rim of the ablation zone are shown in Table 1. The long-axis diameters of the ablation lesions obtained from the samples receiving embolization were significantly longer than those of controls (27.2, 30.2, 28.2, 32.0, and 23.2 mm in Groups A, B, C, D, and controls, respectively) ($P < 0.05$); and the long-axis diameters of Group D was significantly longer than those of both Groups A and C ($P < 0.05$). The short-axis diameters of the ablation lesions obtained from the samples receiving embolization were significantly longer than those of controls (23.2, 26.0, 22.2, 24.4, and 18.5 mm in Groups A, B, C, D, and controls, respectively) ($P < 0.05$). The circularities of the ablation area were not different among the groups. The average diameters of the surrounding hemorrhagic rim in Groups B (3.5 mm), C (4.4 mm), and D (5.8 mm) were significantly longer than

Table 1. Dimensions of the radiofrequency ablation lesion and total application time

Group (no. of lesions)	Long axis (mm)	Short axis (mm)	Circularity	Rim width (mm)	Radiofrequency application time (s)
Control (n = 10)	23.2 ± 1.4	18.5 ± 2.0	0.8 ± 0.1	1.8 ± 0.6	426 ± 125
Group A (n = 6)	27.2 ± 1.6†‡	23.2 ± 2.6†	0.9 ± 0.1	2.5 ± 0.6‡	276 ± 33†
Group B (n = 6)	30.2 ± 1.8†	26.0 ± 2.6†	0.9 ± 0.1	3.5 ± 1.4†‡	279 ± 59†
Group C (n = 8)	28.2 ± 1.9†‡	22.2 ± 2.3†	0.8 ± 0.1	4.4 ± 0.8†‡	291 ± 45†
Group D (n = 8)	32.0 ± 2.6†	24.4 ± 2.8†	0.8 ± 0.1	5.8 ± 1.1†	334 ± 67†

Circularity was calculated to describe the roundness of the radiofrequency ablation zone [30]; radiofrequency application time was calculated as the sum of the duration of the first and second phases of ablation

Control, radiofrequency ablation alone; Group A, radiofrequency ablation was performed just after embolization with gelatin sponge; Group B, radiofrequency ablation was performed just after embolization with iodized oil followed by gelatin sponge; Group C, radiofrequency ablation was performed just after embolization with 700–900 μm microspheres; Group D, radiofrequency ablation was performed just after embolization with 100–300 μm microspheres

† $P < 0.05$ compared to the non-embolization group (control)

‡ $P < 0.05$ compared to Group D

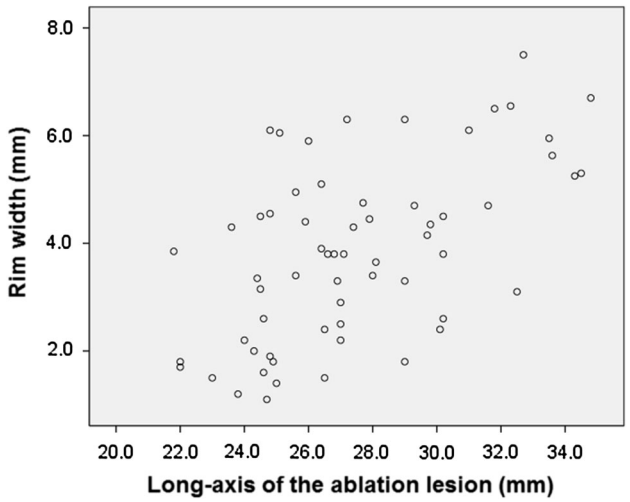

Fig. 1. Correlation between the long-axis of the ablation lesion and the hemorrhagic rim width. These measurements showed significant correlation (Pearson's $r = 0.564$, $P < 0.001$).

that of controls (1.8 mm) ($P < 0.05$); that in Group D was the widest among the groups. The diameters of the hemorrhagic rim significantly correlated with the length of the long-axis in the ablation lesion ($r = 0.564$, $P < 0.01$) (Fig. 1). The average total radiofrequency application time in the embolization groups were significantly shorter than that in the controls (276, 279, 291, 334, and 426 s for Groups A, B, C, D, and controls, respectively) ($P < 0.05$) (Table 1).

Pathologic analysis

All ablation areas included a central coagulation zone with a surrounding hemorrhagic rim (Fig. 2). In the central coagulation zone, a core of ablated, tan to charcoal gray tissue was seen. Macroscopic findings were not different among groups. Microscopic examination revealed that the hepatocytes were changed to dense basophilic nuclei with eosinophilic-stained cytoplasm in the central zone, indicating coagulative necrosis (Fig. 3). The injected microspheres were visible in small venules in Groups C and D (Fig. 4). Some of the microspheres detected within the ablation area were destroyed in the particles. In the surrounding hemorrhagic rim, there were many infiltrated lymphocytes adjacent to hepatocytes with marked hemorrhage. In the peripheral infarction zone seen in four of the six ablation lesions in Group B, sinusoidal dilatation and marked intralobular congestion in the terminal hepatic venules and portal veins were observed.

Discussion

This is the first study to our knowledge to evaluate the enhancement of the radiofrequency ablation-induced coagulation area immediately after embolization using various embolic agents, including gelatin sponge, iodized oil followed by gelatin sponge, 100–300 μm calibrated microspheres, and 700–900 μm calibrated microspheres. All of these enhancements provided a larger necrotic area with a shorter radiofrequency application time compared to radiofrequency ablation alone. When comparing the calibrated microspheres, embolization with use of small (100–300 μm) microspheres induced more extensive effects in the lesion size than did large (700–900 μm) microspheres.

In patients with medium or large-sized HCC, embolization before radiofrequency ablation is beneficial in that it enables a larger volume of necrosis than radiofrequency ablation alone [9], because the efficacy of radiofrequency ablation is based on heat delivery [8, 11]. Moreover, radiofrequency ablation combined with embolization using iodized oil in addition to a gelatin sponge resulted in a larger necrotic area than radiofrequency ablation combined with embolization with a gelatin sponge alone or iodized oil alone [10]. Recent advances have enabled the use of calibrated, small microspheres with various diameters for embolization/chemoembolization for HCC [16, 22]. However, whether the size of the microsphere affects the enhancement of the ablation area has not been clarified. A recent report on the effectiveness of embolization with calibrated microspheres followed by radiofrequency ablation in animal models showed that very small (40 μm) microspheres enhanced radiofrequency ablation size more than did larger ones [17]; these findings support the results of the current study. On the other hand, another study previously found that radiofrequency ablation combined with the use of iodized oil followed by gelatin sponge resulted in the largest area of coagulative necrosis compared to the use of either the gelatin sponge or iodized oil alone [15]. There have been no previous evaluations of the effects of small microspheres compared to iodized oil followed by gelatin sponge, as we did here. Results from the current study indicated that the coagulation dimensions of the radiofrequency ablation combined with small microspheres or iodized oil followed by gelatin sponge were similar in size, and no statistical difference was found between these two groups.

The coagulation area after radiofrequency ablation combined with iodized oil followed by gelatin sponge possibly extended into the peripheral liver parenchyma adjacent to the radiofrequency ablation central lesion [15]. In a previous study, in the short-term after radiofrequency ablation with embolization, these peripheral areas showed a large hemorrhagic area; within a week after the radiofrequency ablation with embolization, this became a large coagulative necrosis area that might be made by a segmental infarction [23]. Preliminary animal studies showed that pretreatment for dual occlusion of the hepatic artery and portal vein resulted in the largest

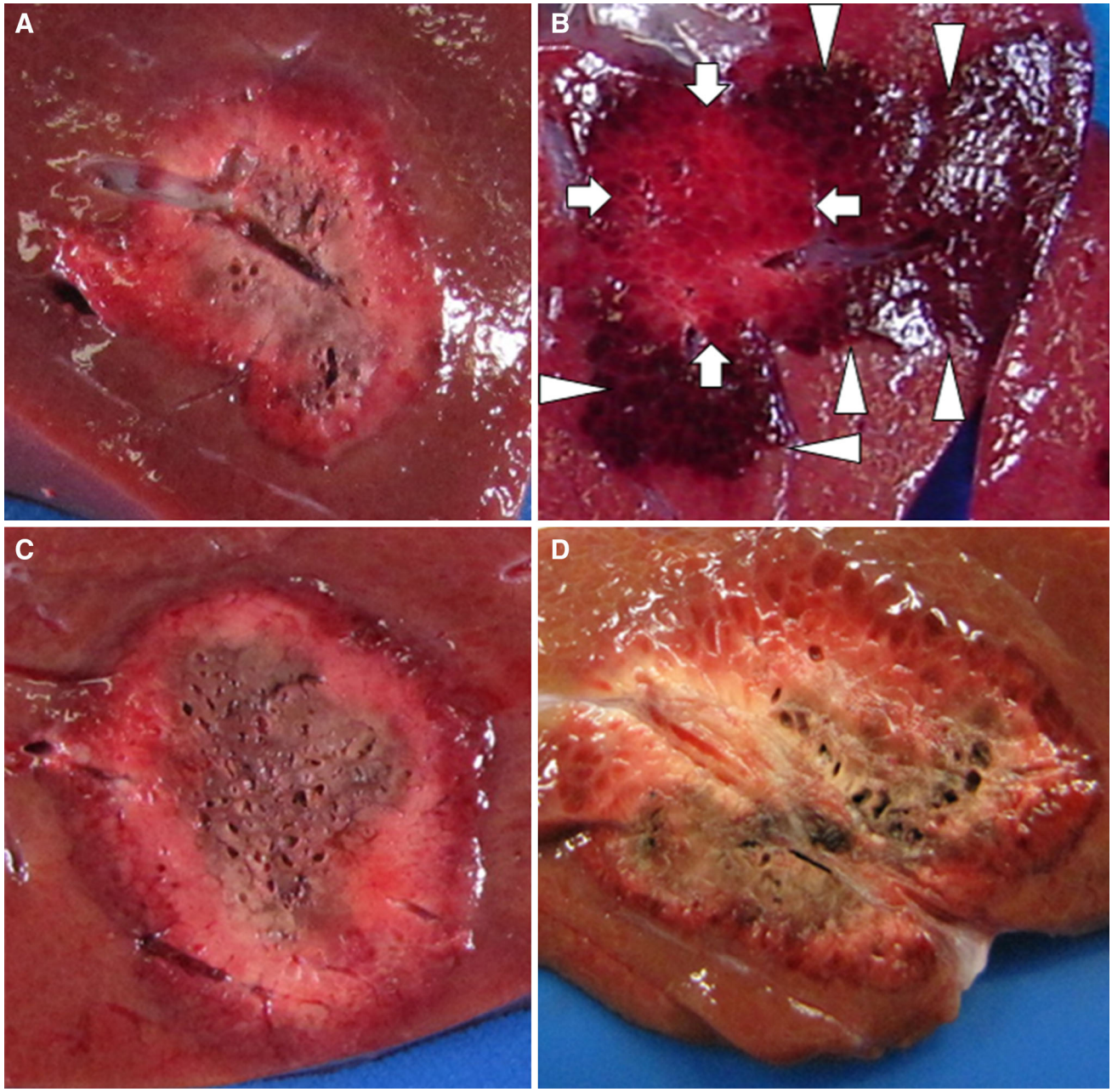

Fig. 2. Gross examination of the radiofrequency ablation lesions with or without combined embolization. **A** Non-embolization control: in the central coagulation zone, a core of ablated tan to charcoal gray tissue was seen. **B** Embolization with iodized oil followed by gelatin sponge: a dark segmental hemorrhagic area (*arrow heads*) toward the periphery of the liver adjacent to the ablation center (*arrows*). **C** Embolization with 100–300 μm microspheres: a central coagulation zone and adjacent hemorrhagic rim are seen. These findings are similar to those in the controls. **D** Embolization with 700–900 μm microspheres: a central coagulation zone and adjacent hemorrhagic rim are seen. These findings are similar to those in the controls.

necrosis lesion induced by radiofrequency ablation [24, 25]. The hypothesis for the phenomenon is that the iodized oil introduced into the hepatic artery would reach the portal vein through the peribiliary arterial plexus, using artery-to-portal-vein communication [26]. Tanaka et al. reported that this segmental infarction area could be produced in an animal liver model of radiofrequency ablation followed by calibrated microspheres [17]. However, contrary to that report, in the current study, none of the 16 lesions from radiofrequency ablation followed by embolization with calibrated microspheres showed this phenomenon. We hypothesize that these

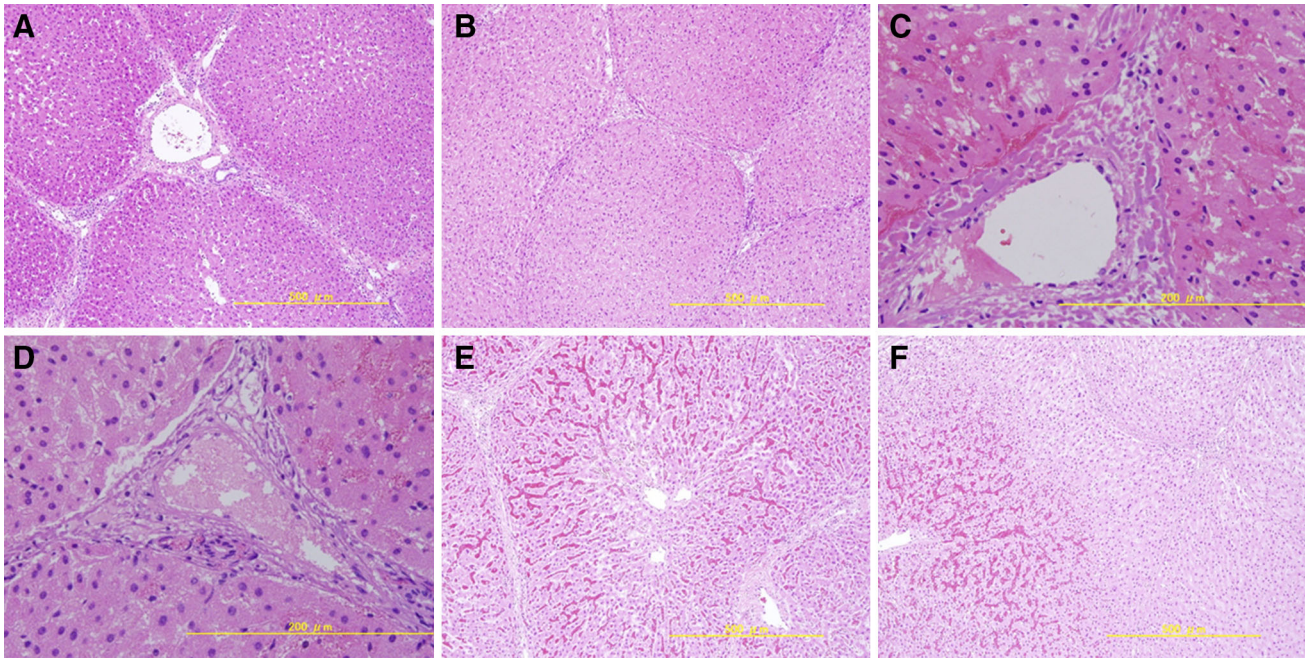

Fig. 3. Hematoxylin and eosin staining of liver samples immediately after radiofrequency ablation with or without combined embolization. **A** Non-ablated liver parenchyma obtained from control animals (non-embolization) (original magnification ×10). **B** Low magnification (original magnification ×10) of the lesions that were embolized with 100–300 μm microspheres followed by radiofrequency ablation. **C** High magnification (original magnification ×40) of the lesions that were embolized with 100–300 μm microspheres followed by radiofrequency ablation. This shows homogenous eosinophilic staining of the cytoplasm and dense homogeneous basophilic staining of the nuclei of hepatocytes, indicating coagulative necrosis. **D** High magnification (original magnification ×40) of the lesions that were embolized with 700–900 μm microspheres followed by radiofrequency ablation. This also shows coagulative necrosis. **E** Hemorrhagic rim surrounding the central coagulation zone after embolization with 100–300 μm microspheres followed by radiofrequency ablation (original magnification ×10). Marked hemolysis is visible in the sinusoids. **F** Hemorrhagic rim (*left side* of the figure) and ablated coagulation area (*right side* of the figure) from the specimens that were ablated after embolization with 700–900 μm microspheres (original magnification ×10).

discrepancies may be due to the size of the microspheres. A 100–300 μm microsphere might not be able to pass the peribiliary arterial plexus, because the size of the peribiliary arterial plexus was reported to be 20 μm in a mouse model [27].

The width of the hemorrhagic rim surrounding the ablation lesion was wider in the specimens that received embolization than in those that received ablation alone; moreover, the width correlated with the length of the long-axis of the central ablation zone. The hemorrhagic rim corresponds to an early inflammatory reaction to the central necrotic tissue [28]; thus, we hypothesize that small embolic agents or iodized oil followed by gelatin sponge provided strong embolization effects to the liver tissue, i.e., strong reductions in the "heat-sink" effect, that resulted in a large ablation area with a wide hemorrhagic rim. At the same time, the present data showed that the average of the total radiofrequency application time in the embolization groups was significantly shorter than that for the control group, suggesting that only a small amount of radiofrequency energy may be needed to complete ablation [28, 29].

The present study may have limitations, such as that a small number of animals and only two sizes of the calibrated microspheres were used. We did not evaluate very small-sized microspheres (under 100 μm), drug-eluting microspheres, or chemotherapeutic agents mixed into the iodized oil (as is done in clinical settings). Furthermore, the vessels embolized in this study were normal, healthy vessels rather than tumor vessels within a cirrhotic liver with abnormal vessels, because there are some difficulties in inducing cirrhosis and hepatic tumors in a pig model. Therefore, the results of this animal model study may not be representative of clinical situations involving treatment of HCC. Further research is needed before applying this combination procedure to human HCC patients.

In conclusion, this experimental study demonstrated that radiofrequency ablation immediately after embolization using calibrated microspheres or iodized oil

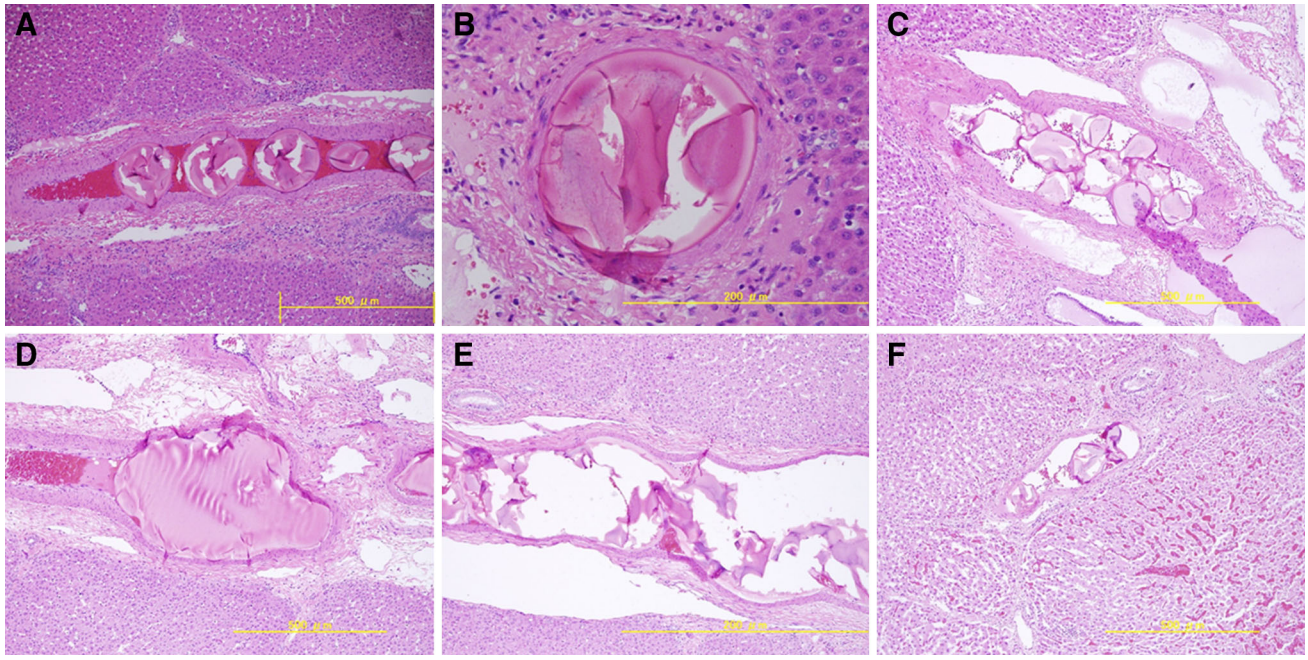

Fig. 4. Hematoxylin and eosin staining of the ablation lesion and peripheral non-ablated parenchyma. **A** Small microspheres are visible within the artery in the non-ablated periphery area adjacent to the radiofrequency ablation zone obtained from animals in Group D (original magnification ×10). **B** High magnification indicates that these microspheres show eosinophilic structures without any inflammatory reactions adjacent to surrounding liver tissue obtained from animals in Group D (original magnification ×40). **C** Broken pieces of the microspheres are seen in the peripheral parenchymal area obtained from animals in Group D (original magnification ×10). **D** Large microspheres are visible within the artery in the non-ablated periphery zone obtained from animals in Group C (original magnification ×10). **E** Broken pieces of the microspheres are seen within the artery obtained from animals in Group C (original magnification ×10). **F** Small microspheres in the hemorrhagic rim area obtained from animals in Group D (original magnification ×10).

followed by gelatin sponge extended the effects on the ablation-induced coagulation size. Smaller microspheres may produce a greater reduction in the "heat-sink" effect on liver tissue than do the larger microspheres.

Compliance with Ethical Standards All applicable international, national, and/or institutional guidelines for the care and use of animals were followed. All procedures performed in studies involving animals were in accordance with the ethical standards of the institution or practice at which the studies were conducted. This article does not contain any studies with human participants performed by any of the authors.

Conflict of interest The authors declare that they have no conflict of interest.

References

1. Bruix J, Sherman M (2005) Management of hepatocellular carcinoma. Hepatology 42:1208–1236
2. Goldberg SN, Gazelle GS, Solbiati L, et al. (1998) Ablation of liver tumors using percutaneous RF therapy. AJR Am J Roentgenol 170:1023–1028
3. Rossi S, Di Stasi M, Buscarini E, et al. (1995) Percutaneous radiofrequency interstitial thermal ablation in the treatment of small hepatocellular carcinoma. Cancer J Sci Am 1:73–81
4. Livraghi T, Goldberg SN, Lazzaroni S, et al. (1999) Small hepatocellular carcinoma: treatment with radio-frequency ablation versus ethanol injection. Radiology 210:655–661
5. Llovet JM, Vilana R, Bru C, et al. (2001) Increased risk of tumor seeding after percutaneous radiofrequency ablation for single hepatocellular carcinoma. Hepatology 33:1124–1129
6. Livraghi T, Goldberg SN, Lazzaroni S, et al. (2000) Hepatocellular carcinoma: radio-frequency ablation of medium and large lesions. Radiology 214:761–768
7. Goldberg SN, Hahn PF, Tanabe KK, et al. (1998) Percutaneous radiofrequency tissue ablation: does perfusion-mediated tissue cooling limit coagulation necrosis? J Vasc Interv Radiol 9:101–111
8. de Baere T, Bessoud B, Dromain C, et al. (2002) Percutaneous radiofrequency ablation of hepatic tumors during temporary venous occlusion. AJR Am J Roentgenol 178:53–59
9. Rossi S, Garbagnati F, Lencioni R, et al. (2000) Percutaneous radiofrequency thermal ablation of nonresectable hepatocellular carcinoma after occlusion of tumor blood supply. Radiology 217:119–126
10. Sugimori K, Morimoto M, Shirato K, et al. (2002) Radiofrequency ablation in a pig liver model: effect of transcatheter arterial embolization on coagulation diameter and histologic characteristics. Hepatol Res 24:164–173
11. Yamakado K, Nakatsuka A, Ohmori S, et al. (2002) Radiofrequency ablation combined with chemoembolization in hepatocellular carcinoma: treatment response based on tumor size and morphology. J Vasc Interv Radiol 13:1225–1232
12. Llovet JM, Bruix J (2003) Systematic review of randomized trials for unresectable hepatocellular carcinoma: chemoembolization improves survival. Hepatology 37:429–442
13. Takayasu K, Arii S, Ikai I, et al. (2006) Prospective cohort study of transarterial chemoembolization for unresectable hepatocellular carcinoma in 8510 patients. Gastroenterology 131:461–469
14. Nakamura H, Hashimoto T, Oi H, et al. (1990) Treatment of hepatocellular carcinoma by segmental hepatic artery injection of

adriamycin-in-oil emulsion with overflow to segmental portal veins. Acta Radiol 31:347–349
15. Sugimori K, Nozawa A, Morimoto M, et al. (2005) Extension of radiofrequency ablation of the liver by transcatheter arterial embolization with iodized oil and gelatin sponge: results in a pig model. J Vasc Interv Radiol 16:849–856
16. Stampfl S, Bellemann N, Stampfl U, et al. (2009) Arterial distribution characteristics of Embozene particles and comparison with other spherical embolic agents in the porcine acute embolization model. J Vasc Interv Radiol 20:1597–1607
17. Tanaka T, Isfort P, Braunschweig T, et al. (2013) Superselective particle embolization enhances efficacy of radiofrequency ablation: effects of particle size and sequence of action. Cardiovasc Intervent Radiol 36:773–782
18. Bonomo G, Della Vigna P, Monfardini L, et al. (2012) Combined therapies for the treatment of technically unresectable liver malignancies: bland embolization and radiofrequency thermal ablation within the same session. Cardiovasc Intervent Radiol 35:1372–1379
19. Lewis AL, Dreher MR (2012) Locoregional drug delivery using image-guided intra-arterial drug eluting bead therapy. J Control Release 161:338–350
20. Lencioni R, de Baere T, Burrel M, et al. (2012) Transcatheter treatment of hepatocellular carcinoma with doxorubicin-loaded DC bead (DEBDOX): technical recommendations. Cardiovasc Interv Radiol 35:980–985
21. Sommer CM, Kortes N, Mogler C, et al. (2012) Super-micro-bland particle embolization combined with RF-ablation: angiographic, macroscopic and microscopic features in porcine kidneys. Eur J Radiol 81:1165–1172
22. Bonomo G, Pedicini V, Monfardini L, et al. (2010) Bland embolization in patients with unresectable hepatocellular carcinoma using precise, tightly size-calibrated, anti-inflammatory microparticles: first clinical experience and one-year follow-up. Cardiovasc Interv Radiol 33:552–559
23. Morimoto M, Numata K, Nozawa A, et al. (2010) Radiofrequency ablation of the liver: extended effect of transcatheter arterial embolization with iodized oil and gelatin sponge on histopathologic changes during follow-up in a pig model. J Vasc Interv Radiol 21:1716–1724
24. Aschoff AJ, Merkle EM, Wong V, et al. (2001) How does alteration of hepatic blood flow affect liver perfusion and radiofrequency-induced thermal lesion size in rabbit liver? J Magn Reson Imaging 13:57–63
25. Chinn SB, Lee FT Jr, Kennedy GD, et al. (2001) Effect of vascular occlusion on radiofrequency ablation of the liver: results in a porcine model. AJR Am J Roentgenol 176:789–795
26. Nakanuma Y, Hoso M, Sanzen T, Sasaki M (1997) Microstructure and development of the normal and pathologic biliary tract in humans, including blood supply. Microsc Res Tech 38:552–570
27. Gonda T, Ishida H, Yoshinaga K, Sugihara K (2000) Microvasculature of small liver metastases in rats. J Surg Res 94:43–48
28. Goldberg SN, Gazelle GS, Compton CC, Mueller PR, Tanabe KK (2000) Treatment of intrahepatic malignancy with radiofrequency ablation: radiologic-pathologic correlation. Cancer 88:2452–2463
29. Patterson EJ, Scudamore CH, Owen DA, Nagy AG, Buczkowski AK (1998) Radiofrequency ablation of porcine liver in vivo: effects of blood flow and treatment time on lesion size. Ann Surg 227:559–565
30. Laeseke PF, Lee FT Jr, Sampson LA, van der Weide DW, Brace CL (2009) Microwave ablation versus radiofrequency ablation in the kidney: high-power triaxial antennas create larger ablation zones than similarly sized internally cooled electrodes. J Vasc Interv Radiol 20:1224–1229

論 文 目 録

Ⅰ 主 論 文

Enhancement of radiofrequency ablation of the liver combined with transarterial embolization using various embolic agents

Kuniyasu Irie, Manabu Morimoto, Kazushi Numata, Masaaki Kondo, Satoshi Moriya, Yu Shimoyama, Akito Nozaki, Yoshihiro Goda, Satoshi Kobayashi, Makoto Ueno, Shinichi Ohkawa, Katsuaki Tanaka, Shin Maeda: Abdom Imaging (2015) 40:1821–1828

Ⅱ 副 論 文　なし

Ⅲ 参 考 論 文 なし